Electronic Supplementary Material (ESI) for Inorganic Chemistry Frontiers.

$Y_2(Te_4O_{10})(SO_4)$: A New Sulfate Tellurite with a Unique Te_4O_{10} Polyanion and Large Birefringence

Peng-Fei Li[a,c], Chun-Li Hu[a], Fang Kong[*,a], Shao-Ming Ying[*,b], Jiang-Gao Mao[a]

[a] *State Key Laboratory of Structural Chemistry, Fujian Institute of Research on the Structure of Matter, Chinese Academy of Sciences, Fuzhou 350002, P. R. China.*

[b] *Fujian Provincial Key Laboratory of Featured Materials in Biochemical Industry, Ningde Normal University, Ningde 352100, P. R. China*

[c] *College of Chemical Engineering, Fuzhou University, Fuzhou, Fujian 350116, P. R. China.*

E-mail: kongfang@fjirsm.ac.cn; ysm@ndnu.edu.cn

Supporting Information

Table S1 Calculated bond valences for compounds $Y_3(TeO_3)_2(SO_4)_2(OH)(H_2O)$ and $Y_2Te_4O_{10}(SO_4)$.

Compound	Bond	Bond lengths	Bond-valence	BVS
$Y_3(TeO_3)_2(SO_4)_2(OH)(H_2O)$	Te(1)-O(1)	1.847(5)	1.421	4.118
	Te(1)-O(2)	1.874(4)	1.321	
	Te(1)-O(3)	1.859(5)	1.376	
	Y(1)-O(1)#1	2.353(5)	0.405	3.300
	Y(1)-O(1)#2	2.353(5)	0.405	
	Y(1)-O(3)	2.267(5)	0.512	
	Y(1)-O(3)#3	2.267(5)	0.512	
	Y(1)-O(4)	2.442(6)	0.319	
	Y(1)-O(5)	2.322(7)	0.441	
	Y(1)-O(8)#4	2.404(5)	0.353	
	Y(1)-O(8)#5	2.404(5)	0.353	
	Y(2)-O(1)#1	2.336(4)	0.425	3.242
	Y(2)-O(2)	2.401(5)	0.356	
	Y(2)-O(2)#6	2.290(5)	0.481	
	Y(2)-O(3)	2.405(5)	0.352	
	Y(2)-O(4)	2.317(10)	0.441	
	Y(2)-O(6)	2.449(5)	0.313	
	Y(2)-O(7)#7	2.307(5)	0.459	
	Y(2)-O(9)#6	2.344(5)	0.415	
	S(1)-O(6)	1.487(6)	1.448	6.102
	S(1)-O(7)	1.460(5)	1.558	
	S(1)-O(8)	1.485(4)	1.456	
	S(1)-O(9)	1.441(5)	1.640	
$Y_2Te_4O_{10}(SO_4)$	Te(1)-O(1)	1.863(7)	1.361	3.984
	Te(1)-O(2)	1.909(8)	1.202	
	Te(1)-O(3)	1.847(8)	1.421	
	Te(2)-O(3)#1	2.495(8)	0.247	4.134
	Te(2)-O(4)	1.855(7)	1.391	
	Te(2)-O(5)	1.864(8)	1.357	
	Te(2)-O(6)	1.929(8)	1.139	
	Te(3)-O(6)#2	1.943(8)	1.096	4.021
	Te(3)-O(7)	1.863(7)	1.361	
	Te(3)-O(8)	1.883(8)	1.289	
	Te(3)-O(9)#3	2.454(7)	0.275	
	Te(4)-O(1)#4	2.336(8)	0.379	4.128
	Te(4)-O(2)#5	2.020(8)	0.890	
	Te(4)-O(9)	1.870(8)	1.335	

	Te(4)-O(10)	1.821(8)	1.524	
	Y(1)-O(3)#1	2.358(8)	0.400	2.962
	Y(1)-O(4)#6	2.354(7)	0.404	
	Y(1)-O(5)	2.401(8)	0.356	
	Y(1)-O(7)	2.436(8)	0.324	
	Y(1)-O(8)#7	2.357(8)	0.401	
	Y(1)-O(9)#3	2.473(7)	0.293	
	Y(1)-O(11)	2.314(8)	0.451	
	Y(1)-O(12)#3	2.426(8)	0.333	
	Y(2)-O(1)#1	2.389(8)	0.368	3.101
	Y(2)-O(4)	2.272(7)	0.505	
	Y(2)-O(5)#2	2.331(8)	0.430	
	Y(2)-O(7)	2.297(7)	0.472	
	Y(2)-O(8)#8	2.464(7)	0.300	
	Y(2)-O(9)#9	2.441(7)	0.320	
	Y(2)-(10)#10	2.148(8)	0.706	
	S(1)-O(11)	1.456(8)	1.575	6.108
	S(1)-O(12)	1.487(8)	1.448	
	S(1)-O(13)	1.448(9)	1.609	
	S(1)-O(14)	1.480(8)	1.476	

Symmetry transformations used to generate equivalent atoms:

For $Y_3(TeO_3)_2(SO_4)_2(OH)(H_2O)$: #1 x-1, y, z #2 x-1, -y+3/2, z #3 x, -y+3/2, z
#4 -x-1, -y+1, -z+1 #5 -x-1, y+1/2, -z+1 #6 -x, -y+1, -z+2 #7 -x-1, -y+1, -z+2

For $Y_2Te_4O_{10}(SO_4)$: #1 -x+1, -y+1, -z+1 #2 -x+1, -y+1, -z+2 #3 -x, -y+2, -z+2
#4 x, y+1, z+1 #5 x-1, y+1, z+1 #6 x-1, y, z #7 -x, -y+1, -z+2 #8 x+1, y, z
#9 -x+1, -y+2, -z+2 #10 x+1, y-1, z-1

Table S2 Band gaps of some reported yttrium tellurites.

Compounds	Space Group	Eg (eV)	Ref.
$YVTe_2O_8$	***C2/m***	2.2	8
$CsYTe_3O_8$	***R-3***	3.4	6
$YNbTe_2O_8$	***C2/m***	3.4	5
$RbY(TeO_3)_2$	***Pnma***	3.6	6
$KY(TeO_3)_2$	***Pnma***	3.8	6
$NaYTe_4O_{10}$	***P4₂/nbc***	3.9	6
$Y_2(Te_4O_{10})(SO_4)$	***P-1***	4.10	This work
$Na_2Y_3Cl_3(TeO_3)_4$	***C2/c***	4.26	7
$Y_3(TeO_3)_2(SO_4)_2(OH)(H_2O)$	***P2₁/m***	4.40	This work

Table S3 State energies (eV) of the lowest conduction band and the highest valence band of $Y_3(TeO_3)_2(SO_4)_2(OH)(H_2O)$ and $Y_2(Te_4O_{10})(SO_4)$.

Compound	k-point	L-CB	H-VB
$Y_3(TeO_3)_2(SO_4)_2$ $(OH)(H_2O)$	Z (0.000, 0.000, 0.500)	1.710489	-0.12089
	G (0.000, 0.000, 0.000)	1.892469	-0.13787
	Y (0.000, 0.500, 0.000)	1.962409	-0.15599
	A (-0.500, 0.500, 0.000)	2.096052	-0.00904
	B (-0.500, 0.000, 0.000)	2.080662	0
	D (-0.500, 0.000, 0.500)	1.892063	-0.01012
	E (-0.500, 0.500, 0.500)	1.890435	-0.02000
	C (0.000, 0.500, 0.500)	1.738010	-0.14745
$Y_2(Te_4O_{10})(SO_4)$	G (0.000, 0.000, 0.000)	3.659691	-0.00043
	F (0.000, 0.500, 0.000)	3.845670	-0.07314
	Q (0.000, 0.000, 0.500)	3.815348	0
	Z (0.000, 0.000, 0.500)	3.747897	-0.06240
	G (0.000, 0.000, 0.000)	3.659691	-0.00043

Computational Method

Single-crystal structural data of compounds $Y_3(TeO_3)_2(SO_4)_2(OH)(H_2O)$ and $Y_2(Te_4O_{10})(SO_4)$ were used for the theoretical calculations. The electronic structures were performed using a plane-wave basis set and pseudo-potentials within density functional theory (DFT) implemented in the total-energy code CASTEP **[**1**]**. For the exchange and correlation functional, we chose Perdew–Burke–Ernzerhof (PBE) in the generalized gradient approximation (GGA) **[**2**]**. The interactions between the ionic cores and the electrons were described by the ultrasoft pseudopotential **[**3**]**. The following valence-electron configurations were considered in the computation: Y-$4d^1 4p^6 5s^2$, Te-$5s^2 5p^4$, O-$2s^2 2p^4$, S-$3s^2 3p^4$ and H-$1s^1$. The numbers of plane waves included in the basis sets were determined by cutoff energy of 750 eV and 340 eV for $Y_3(TeO_3)_2(SO_4)_2(OH)(H_2O)$ and $Y_2(Te_4O_{10})(SO_4)$ respectively. The numerical integration of the Brillouin zone was performed using Monkhorst-Pack k-point sampling of 4 × 3 × 3 for $Y_3(TeO_3)_2(SO_4)_2(OH)(H_2O)$ and $Y_2(Te_4O_{10})(SO_4)$ respectively. The other parameters and convergent criteria were the default values of CASTEP code.

The calculations of linear optical properties in terms of the complex dielectric function $\varepsilon(\omega) = \varepsilon_1(\omega) + i\varepsilon_2(\omega)$ were made. The imaginary part of the dielectric function ε2 was given in the following equation:

$$\varepsilon^{ij}_2(\omega) = \frac{8\pi^2 h^2 e^2}{(m^2 V)} \sum_k \sum_{cv} (f_c - f_v) \frac{p^i_{cv}(k) p^j_{cv}(k)}{E^2_{vc}} \delta\, [E_c(\mathrm{k}) - E_v(\mathrm{k}) - h\omega]$$

The f_c and f_v represent the Fermi distribution functions of the conduction and valence band. The term $p^i_{cv}(k)$ denotes the momentum matrix element transition from the energy level c of the conduction band to the level v of the valence band at the *k*th point in the Brillouin zone (BZ), and *V* is the volume of the unit cell.

The real part $\varepsilon_1(\omega)$ of the dielectric function $\varepsilon(\omega)$ follows from the Kramer–Kronig relationship. All the other optical constants may be derived from $\varepsilon_1(\omega)$ and $\varepsilon_2(\omega)$. For example, the refractive index n(ω) can be calculated using the following expression[4]:

$$n(\omega)=\left(\frac{1}{\sqrt{2}}\right)\left[\sqrt{\varepsilon_1^2(\omega)+\varepsilon_2^2(\omega)}+\varepsilon_1(\omega)\right]^{1/2}$$

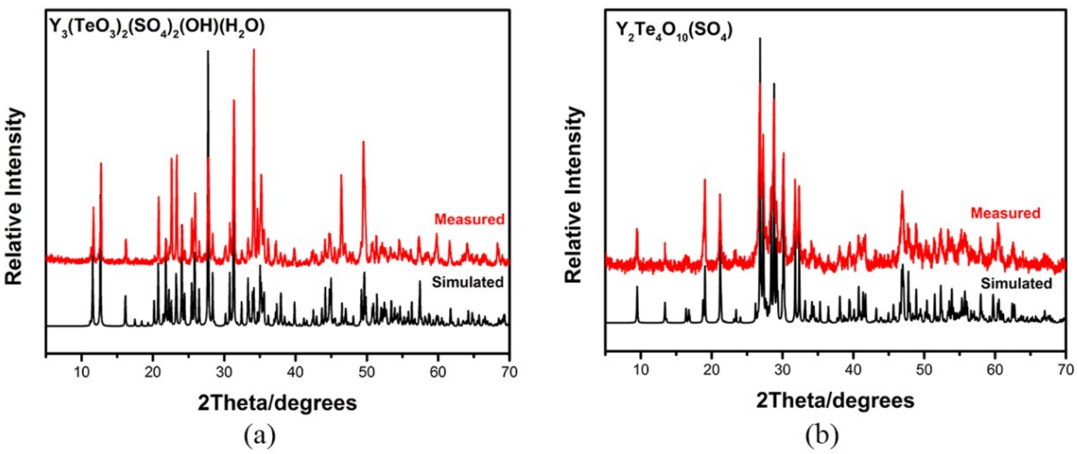

Figure S1. Simulated and experimental powder X-ray diffractometer patterns of $Y_3(TeO_3)_2(SO_4)_2(OH)(H_2O)$ (a) and $Y_2(Te_4O_{10})(SO_4)$ (b).

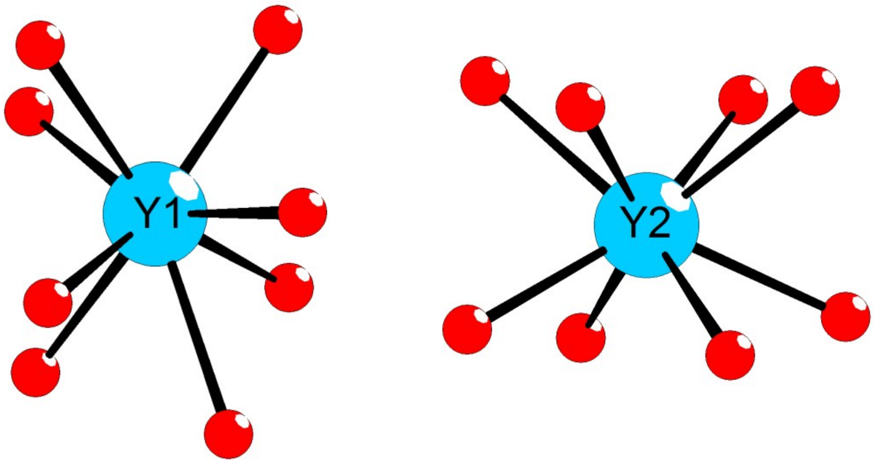

Figure S2 Coordination modes of Y(1) and Y(2) in $Y_3(TeO_3)_2(SO_4)_2(OH)(H_2O)$.

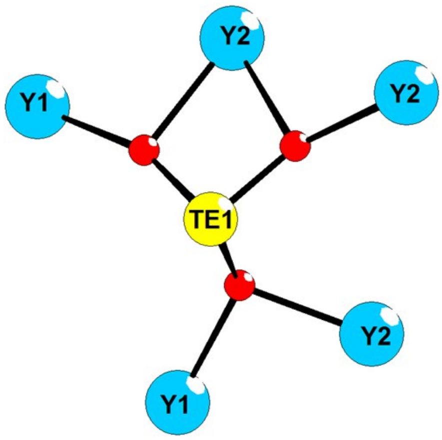

Figure S3 Coordination environment of $Te(1)O_3$ group in $Y_3(TeO_3)_2(SO_4)_2(OH)(H_2O)$.

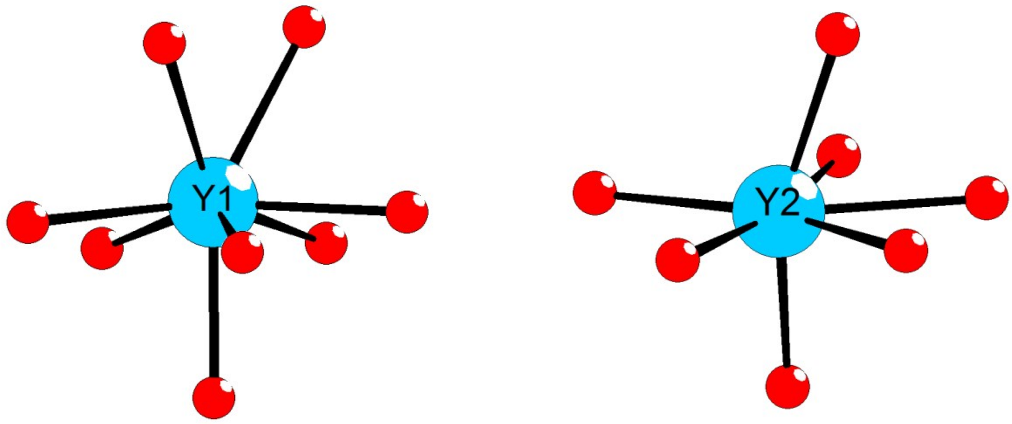

Figure S4 Coordination modes of Y(1) and Y(2) in $Y_2(Te_4O_{10})(SO_4)$.

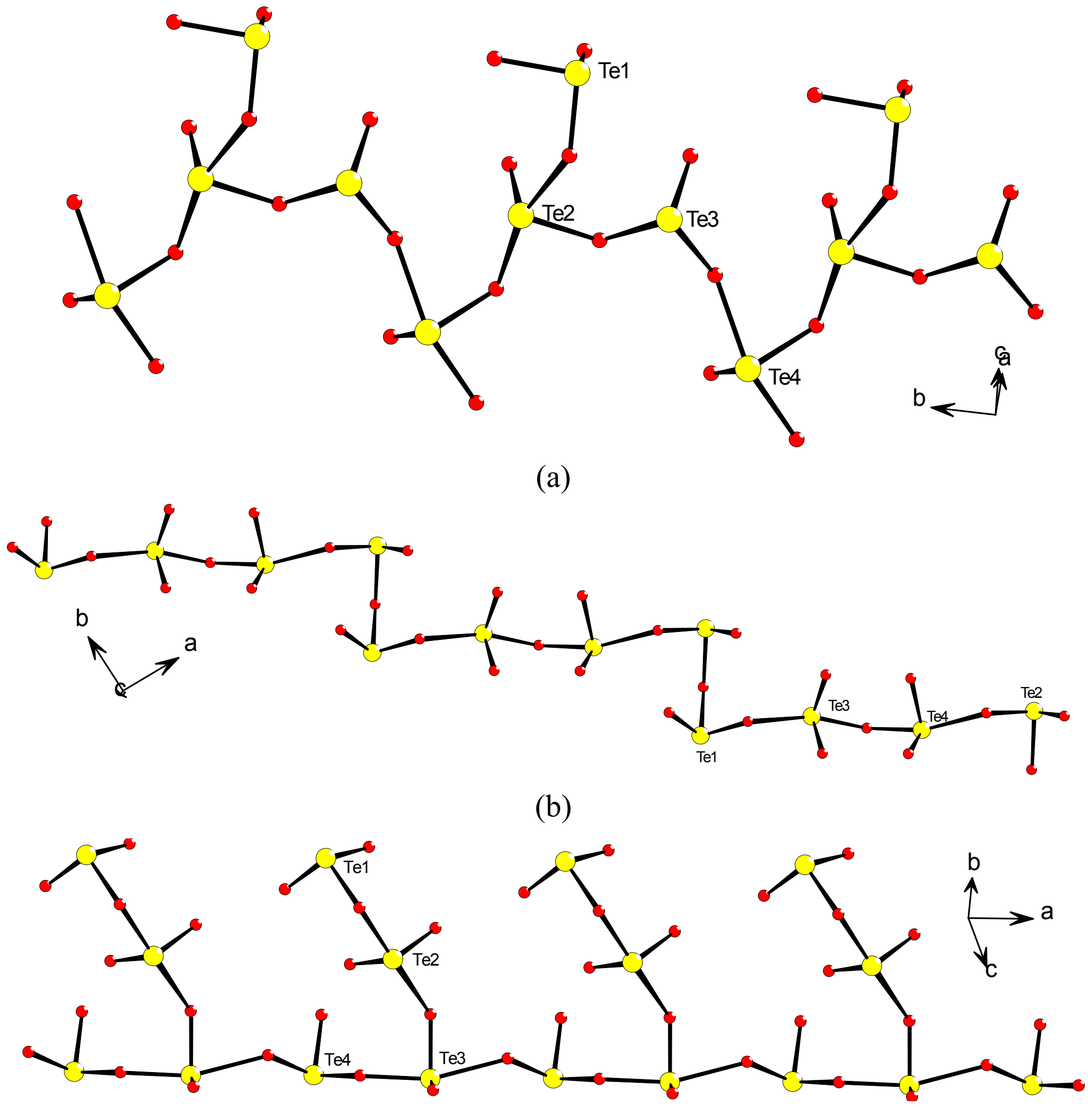

(a)

(b)

(c)

Figure S5 $(Te_4O_{10})^{4-}$ 1D polyanionic chains in $Ba_2(VO_3)[Te_4O_9(OH)]$ (a), $HoCl(Te_2O_5)$(b) and $Nd_2(MoO_4)(Te_4O_{10})$ (c).

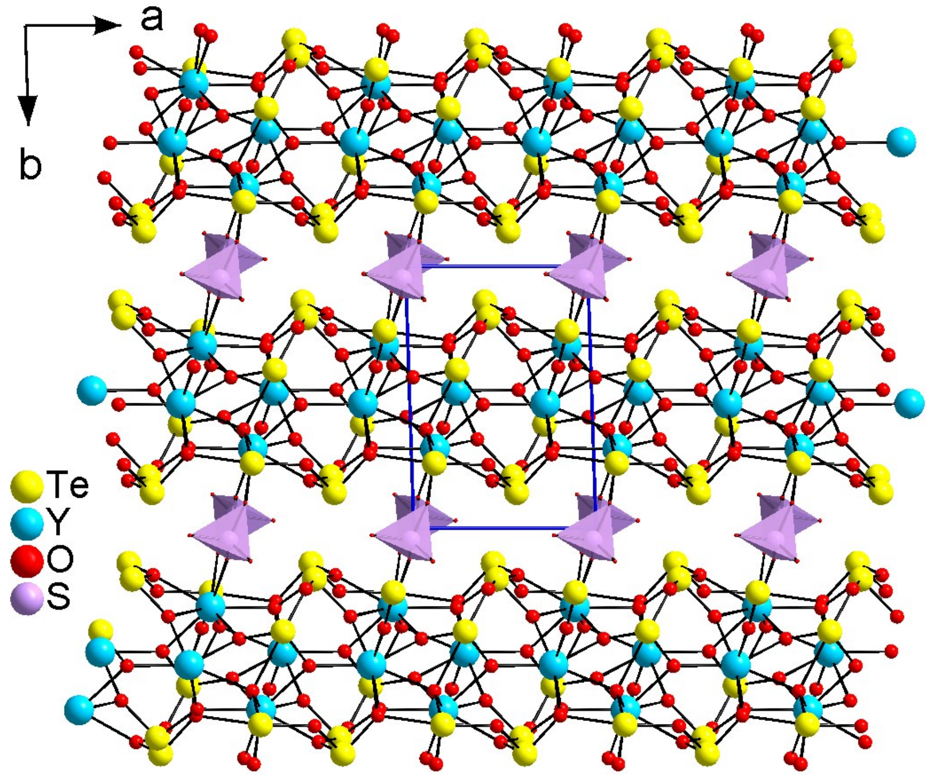

Figure S6 View of the structure of $Y_2(Te_4O_{10})(SO_4)$ along c-axis.

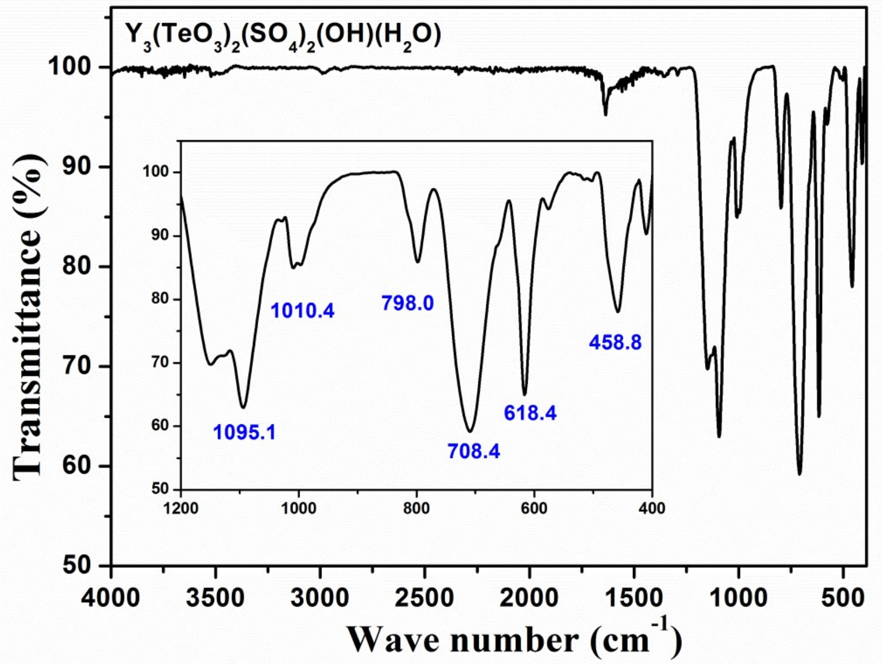

(a)

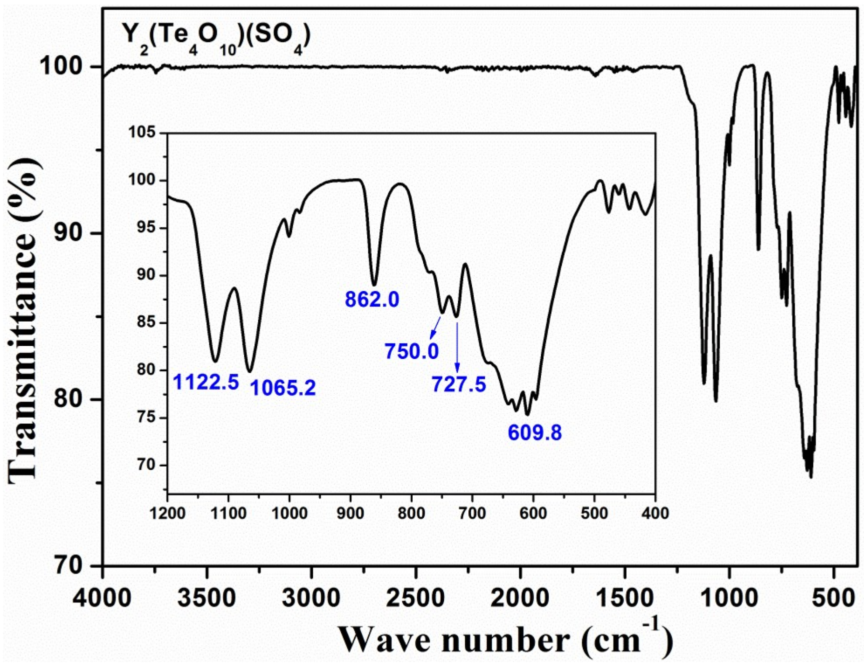

(b)

Figure S7. IR spectra of $Y_3(TeO_3)_2(SO_4)_2(OH)(H_2O)$ (a) and $Y_2(Te_4O_{10})(SO_4)$ (b).

References

[1] M. D. Segall, P. J. D. Lindan, M. J. Probert, C. J. Pickard, P. J. Hasnip, S. J. Clark and M. C. J. Payne, First-principles simulation: ideas, illustrations and the CASTEP code, *Phys-Condens Mat.*, 2002, **14**, 2717.

[2**]** V. Milman, B. Winkler, J. A. White, C. J. Pickard, M. C. Payne, E. V. Akhmatskaya and R. H. Nobes, Electronic structure, properties, and phase stability of inorganic crystals: A pseudopotential plane-wave study, *Int. J. Quantum. Chem.*, 2000, **77**, 895-910.

[3**]** J. P. Perdew, K. Burke and M. Ernzerhof, Generalized Gradient Approximation Made Simple, *Phys. Rev. Lett.*, 1996, **77**, 3865.

[4**]** S. Saha and T. P. Sinha, Electronic structure, chemical bonding, and optical properties of paraelectric $BaTiO_3$, 2000, **62**, 8828-8834.

[5] Y. H. Kim, B. Y. Jeon, T. S. You and K. M. Ok, New quaternary oxides with both families of second-order Jahn–Teller (SOJT) distortive cations: Solid-state synthesis, structure determination, and characterization of $YNbTe_2O_8$ and $YNbSe_2O_8$, *J. Alloy. Compd.*, 2015, **637**, 155-161.

[6] Y. Kim, D. W. Lee and K. M. Ok, Rich Structural Chemistry in New Alkali Metal Yttrium Tellurites: Three-Dimensional Frameworks of $NaYTe_4O_{10}$, $KY(TeO_3)_2$, $RbY(TeO_3)_2$, and a Novel Variant of Hexagonal Tungsten Bronze, $CsYTe_3O_8$, *Inorg. Chem.*, 2015, **54**, 389-395.

[7] S. Zitzer, F. Schleifenbaum and T. Schleid, $Na_2Y_3Cl_3[TeO_3]_4$: Synthesis, Crystal Structure and Spectroscopic Properties of the Bulk Material and its Luminescent Eu^{3+}-doped Samples, *Z. Naturforsch.*, 2014, **69**, 150-158.

[8] Y. H. Kim, D. W. Lee and K. M. Ok, Noncentrosymmetric $YVSe_2O_8$ and Centrosymmetric $YVTe_2O_8$: Macroscopic Centricities Influenced by the Size of Lone Pair Cation Linkers, *Inorg. Chem.*, 2014, **53**, 1250-1256.